2013-2767

44^{th} AIAA Thermophysics Conference, June 2013, San Diego, California.

Porous-material Analysis Toolbox based on OpenFOAM-extend and Applications

Jean Lachaud *

University of California Santa Cruz, Moffett Field, CA

Nagi N. Mansour†

NASA Ames Research Center, Moffett Field, CA

The Porous-material Analysis Toolbox based on OpenFOAM-extend (PATO) is a modular analysis platform specifically implemented to test innovative physics-based models for porous materials submitted to high-temperature environments or other unusual conditions. The governing equations implemented in the different modules are volume-averaged forms of the mass-, momentum-, and energy-conservation equations for porous media. Current developments are focussed on ablative materials. PATO is currently composed of two types of modules: (1) global analysis modules, that may be used to run a full ablative material response, with an applied/macroscopic scale point of view; (2) elementary analysis modules, that may be used to study specific fundamental aspects, with a detailed/microscopic scale point of view. Examples of global and elementary analysis applications are presented: volume-averaged simulation of the oxidation of the fibers in a carbon-fiber preform, multi-dimensional pyrolysis-gas flow in a cylinder facing an arc-jet, comparison of equilibrium and finite-rate chemistry in a carbon/phenolic ablative material.

Nomenclature

A_i	Gaseous species i
A_j	Arrhenius law pre-exponential factor, SI
C_H	Stanton number for heat transfer
C_M	Stanton number for mass transfer
c_p	Specific heat, $J \cdot kg^{-1} \cdot K^{-1}$
e	Specific energy, $J \cdot kg^{-1}$
E_j	Arrhenius law activation energy, $J \cdot kg^{-1}$
F_j	Fraction of mass lost through pyrolysis reaction j
Fo	Forchheimer number
h	Specific enthalpy, $J \cdot kg^{-1}$
j	Diffusive flux, $mol \cdot m^{-2} \cdot s^{-1}$
K	Permeability
K_i	Chemical equilibrium constant for reaction i
l	Thickness or length, m
m_j	Arrhenius law parameter
M_k	Molar mass of species k, $kg \cdot mol^{-1}$
N_g	Number of gaseous species
n_j	Arrhenius law parameter

*Scientist, AIAA Senior Member. SVI/UCSC, NASA Ames Research Park, Building 19, Moffett Field, CA 94035.

†Chief Scientist for Modeling and Simulation, TN Division. AIAA Associate Fellow. NASA Ames Research Center, Building 254, Moffett Field, CA 94035.

N_p Number of pyrolysis reactions
p Pressure, Pa
q Heat flux, $J \cdot m^{-2} \cdot s^{-1}$
R Perfect gas constant, $J \cdot kg^{-1} \cdot K^{-1}$
v Convection velocity, $m \cdot s^{-1}$
y Mass fraction

Greek

β Klinkenberg coefficient, Pa
ϵ Volume fraction
γ_{ji} Stoichiometric coefficient, reaction j species i
μ Viscosity, $Pa \cdot s^1$
ω Reaction rate, $mol \cdot m^{-3} \cdot s^{-1}$
ω^s Solid reaction rate, $mol \cdot m^{-3} \cdot s^{-1}$
Π Pyrolysis gas production rate, $kg \cdot m^{-3} \cdot s^{-1}$
π Molar pyrolysis-gas production rate of species i, $mol \cdot m^{-3} \cdot s^{-1}$
ρ Density, $kg \cdot m^{-3}$
τ Characteristic time, s
τ^s Mechanical erosion rate, $mol \cdot m^{-3} \cdot s^{-1}$
ξ_j Advancement of pyrolysis reaction j

Subscripts

a Ablative material (gas, fiber, and matrix)
c Char
e Boundary layer edge properties
f Reinforcement (non-pyrolyzing phase)
g Gas phase
m, PM Pyrolyzing material
mv Virgin polymer matrix
p Pyrolysis
pg Pyrolysis gas
s Solid phase

Other fonts and operators

$\mathcal{F}_i$ Diffusion flux of the i^{th} species, $kg \cdot m^{-2} \cdot s^{-1}$
$\dot{m}$ Mass flow rate, $kg \cdot m^{-2} \cdot s^{-1}$

$\partial_{\mathbf{x}} \cdot ()$ Divergence
$\partial_t ()$ Time derivative
$\underline{\underline{\mathbf{T}}}$ Second order tensor
$\mathbf{u}$ Vector

I. Introduction

A Porous-material Analysis Toolbox based on OpenFOAM-extend (PATO) is being developed as a fully portable OpenFOAM-Extend library (www.extend-project.de). OpenFOAM is an open-source finite-volume computational-fluid-dynamic software released by OpenCFD Limited (www.opencfd.com). [a] OpenFOAM-extend is a community extension of the official OpenFOAM release. PATO makes use of several OpenFOAM-Extend features.

PATO is a modular analysis platform specifically implemented to test innovative physics-based models for porous materials submitted to high-temperature environments or other unusual conditions. The governing equations implemented in the different modules are volume-averaged forms of the mass-, momentum-, and energy-conservation equations for porous media. While PATO could be used to model any porous material, it is currently developed more specifically for ablative materials. PATO inherits from the flexibility and versatility of OpenFOAM, making it an excellent platform to

[a]The PATO library is not endorsed by OpenCFD Limited, the producer of the OpenFOAM software and owner of the OPENFOAM (R) and OpenCFD (R) trade marks.

- easily and reliably implement and test new models,
- down-select models/mathematical frameworks before implementing them in production codes,
- analyze special configurations and conditions not readily available in production codes.

The objective of this paper is to present the different modules currently available in PATO and a selection of original analyses on the response of porous ablative materials to high-enthalpy environments. In section II, we give an overview of the phenomenology of porous ablative materials. In section III, the volume-averaged mathematical framework for ablative porous materials implemented in PATO is presented. This framework is fully compatible with current state-of-the-art ablation models but adds new models specific to porous media. In section IV, PATO itself is presented: modules available, numerical method, and verification. Then, three original applications/analyses are proposed.

II. Phenomenology of porous ablative materials

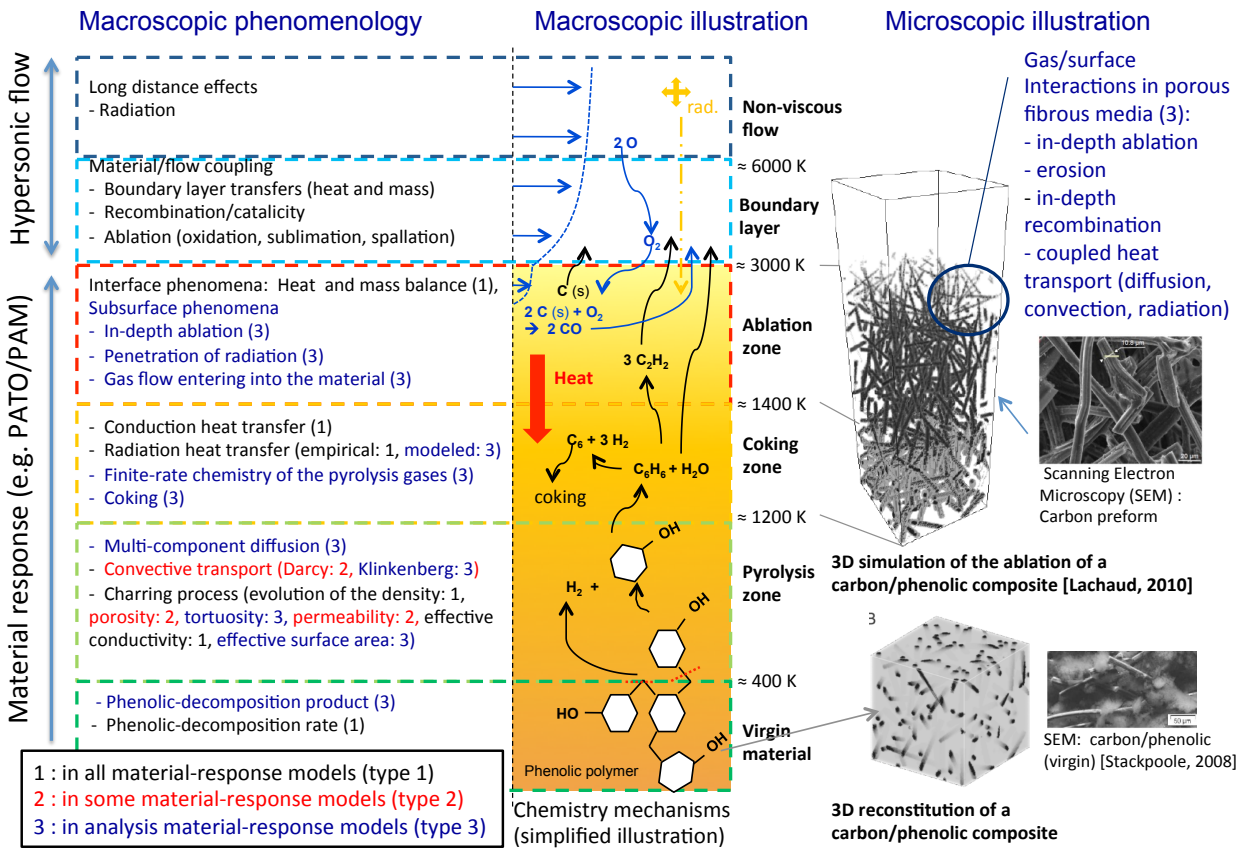

Figure 1. Illustration of the phenomenology of porous ablative materials (a low-density carbon/phenolic ablative material is used as an example)

To illustrate the modeling section, figure 1 puts in perspective in a single chart the following:

- A macroscopic illustration (center) showing the response of a low-density carbon/phenolic ablative materials during atmospheric entry. The virgin material undergoes thermal degradation and ultimately recession captured by the following physico-chemical phenomena [1]:
  - Solid Pyrolysis (pyrolysis zone). The phenolic polymer is thermally decomposed and progressively carbonized into a low density turbostratic graphite, loosing mass while releasing pyrolysis

gases under the form of water, hydrogen, and hydrocarbons [2–4]. To illustrate this process without getting into too much details in this overview, the production of hydrogen and phenol that are two principal products of the pyrolysis are shown in the illustration. Phenol (C_6H_5OH) is schematically represented by a white carbon cycle with an OH group.

  - Pyrolysis-gas Transport and Chemistry (char layer = coking zone and ablation zone). The pyrolysis gases released by solid pyrolysis percolate and diffuse to the surface through the network of pores. Reactions within the pyrolysis gas mixture (homogeneous reactions, e.g. $C_6H_5OH + H_2 \leftrightharpoons C_6H_6 + H_2O$) and between pyrolysis gases and the char take place with possible coking effects (heterogeneous reactions, e.g. $C_6H_6 \leftrightharpoons C_{6(gr)} + 3H_2$). Mixing of the pyrolysis gases with boundary layer gases into the pores of the material occur when boundary layer gases penetrate in the material by forced convection or due to fast diffusion at low pressures.
  - Ablation Chemistry (ablation zone). After charring (and possible coking), the material is removed by ablation and the initial surface recedes. Depending on entry conditions, ablation may be caused by heterogeneous chemical reactions (oxidation, e.g. $2C_{(gr)} + O_2 \leftrightharpoons 2CO$, or sometimes nitridation), phase change (sublimation, e.g. $C_{(gr)} \leftrightharpoons C_{(gas)}$), and possibly mechanical erosion (often called spallation). For porous materials, the thickness of the ablation zone depends on the thermo-chemical conditions and the material microstructure [5].

- A microscopic illustration (right) showing the microscopic (fiber-scale) architecture of the virgin material and its evolution with charring and ablation. The images are scanning electron microscopy (SEM) scans and Direct Numerical Simulations (DNS) at the fiber scale [6]. The microscopic scale simulation are extremely costly in computational time (typically 24 hours on a single processor to simulate the oxidation of a $400\mu m \times 100\mu m \times 100\mu m$ carbon preform during one second [6]) and cannot realistically be used for design or Thermal Protection System (TPS)-response analysis. The fundamental microscopic-scale equations need to be volume-averaged [7] into physics-based macroscopic equations that can be solved more efficiently [8]. PATO includes a suite of tools that can be used to extract intrinsic (microscopic) data (e.g. fiber reactivity) from macroscopic experiments and to guide the development of volume-average models [6].

- A macroscopic summary of the phenomenology (left side of the figure) using the common macroscopic-scale (volume-averaged) nomenclature for the mass, momentum, and energy-conservation terms. A review of the models published in the open literature reveals three levels of coherent models [9]. In the figure, these three levels are represented with different colors (and indexes for black-and-white printed copies). A complete description - in equations - is available in section IV but we wish to provide here a quick overview. The first level, based on the state-of-the-art CMA model, is implemented in all design codes; its phenomenology is described in black and referenced as type (1). The core phenomena of the pyrolysis-ablation problem are modeled but many simplification are used. A major simplification is that the momentum-conservation is not implemented, meaning that the direction of the pyrolysis flux and the internal pressure need to be arbitrarily prescribed by the user. This type (1) model is well adapted for uni-dimensional, quasi-steady-state, and equilibrium or frozen chemistry conditions. The second level includes the implementation of the momentum conservation. This capability is found in a few design codes and in several recent analysis codes [9]. The added terms are described in red and referenced as type (2). In blue and referenced as type (3) are the details of the physical phenomena occurring in a porous carbon/phenolic ablative material. Three-dimensional type 2 and type 3 solvers are available in PATO.

III. First-order volume-averaged mathematical framework for porous ablative materials

This section presents a mathematical framework for porous ablative materials. The governing macroscopic equations to model porous media are volume-averaged forms of the mass, momentum, and energy conservation equations [7]. Current type 1 and 2 state-of-the-art models are based on simplified derivations of these three fundamental equations [9,10]. We present here an exact first-order volume-averaged [7] derivation for a type 3 model and its associated boundary conditions. The proposed mathematical framework has directly been developed for type 3 models but degenerates in state-of-the-art type 1 and type 2 models under

the same physical hypotheses. This layered structure presents a remarkable advantage because new modules can easily and rigorously be compared to heritage models as shown in section V.

The presentation of this section can be followed in parallel in figure 1. We will continue using low-density carbon-phenolic as an example. In other word, we will assume that the material is made of three phases: carbon fibers, phenolic polymer, and gas (in the pores).

III.A. Mass conservation

The gaseous mass-conservation equation includes a production term (right-hand side) to account for the pyrolysis gas production, noted Π, and reads

$$\partial_t(\epsilon_g \rho_g) + \partial_{\mathbf{x}} \cdot (\epsilon_g \rho_g \mathbf{v_g}) = \Pi \tag{1}$$

In all type 1 and in some type 2 codes [9], the time derivative is omitted and the gas flow problem is treated as a succession of steady state problems. This simplification is acceptable when the variations of the intensive variables (temperature, pressure) are slow compared to the characteristic time of the flow in the porous medium [9]. The determination of the direction of the gas velocity, $\mathbf{v_g}$, is necessary to solve the average mass-conservation equation. In type 1 codes, this equation is numerically integrated with the assumption that the gas flow is perpendicular to the surface and directed towards the surface. This is correct for one-dimensional steady-state problems with an impermeable back face; in other configurations, the direction and velocity of the flow has to be determined by resolution of the momentum-conservation equation (see subsection III.B). The pyrolysis gas production - Π - is traditionally obtained by fitting thermogravimetry analysis of the resin decomposition using one or several Arrhenius laws [11]. For example, for phenolic polymers, it has been shown that the pyrolysis degradation process follows four steps [3], that may be described by four heterogeneous decomposition reactions [4]. Therefore, for any pyrolyzing phase within a given ablative material, a convenient notation for $j \in [1, N_p]$ pyrolysis reactions is

$$PM_j \rightarrow \sum_{i=1}^{N_g} \gamma_{ji} A_i \tag{2}$$

where PM_j is a fictive solid species of the pyrolyzing material (PM), that is the phenolic matrix in the case of low-density carbon-phenolic. The pyrolyzing phase density is given by

$$\epsilon_m \rho_m = \epsilon_{mv} \rho_{mv} \sum_{j=1}^{N_p} F_j (1 - \xi_j) \tag{3}$$

where

$$\frac{\partial_t \xi_j}{(1-\xi_j)^{m_j}} = T^{n_j} \mathcal{A}_j \exp\left(-\frac{\mathcal{E}_j}{\mathcal{R}T}\right) \tag{4}$$

The pyrolysis-gas production is given by

$$\Pi = -\partial_t(\epsilon_m \rho_m) = \epsilon_{mv} \rho_{mv} \sum_{j=1}^{N_p} F_j \partial_t(\xi_j) \tag{5}$$

In the literature, the form of the equations used to describe pyrolysis vary but they are all mathematically equivalent. State-of-the-art design codes (type 1 and 2) do not track the species production. Only the average mass production -Π - is computed from the Arrhenius laws. A constant elemental fraction of the pyrolysis gas is assumed. This is known to not be fully correct since the composition of the gases produced by pyrolysis is not constant - it is a function of temperature, heating rate, and possibly pressure [4, 12]. The gas chemical composition and derived quantities (gas enthalpy, viscosity, mean molar mass) are computed assuming chemical equilibrium in general (type 1 and type 2 codes). This assumption is often correct but sometimes leads to a pyrolysis-reaction model that is exothermic instead of being endothermic, as experimentally observed [13]. Heuristic methods that arbitrarily modify the enthalpy of the pyrolysis gases

to obtain a better agreement with experimental observations have been proposed [14]. In this case, the actual gas composition and other properties (viscosity, mean molar mass, diffusion coefficients) are still unknown since the real gas composition is unknown. This is not a problem for type 1 codes that completely ignore these terms. However, the arbitrary modification of the pyrolysis gas enthalpy (without tracking the real gas composition) creates an inconsistency in type 2 codes that make use of the viscosity and mean-molar mass to compute the gas flow direction and the internal pressure. Therefore, for high-fidelity modeling, it is important to experimentally determine not only the elemental composition of the pyrolysis gases but also their molar composition. The pyrolysis gas production rate for each species i could readily be obtained using

$$\pi_i = \epsilon_m \rho_{mv} \sum_{j=1}^{N_p} \left[\partial_t \xi_j \, F_j \, \widetilde{\gamma}_{ji} \right] \tag{6}$$

where

$$\widetilde{\gamma}_{ji} = \frac{\gamma_{ji}}{\sum_{k=1}^{N_g} \gamma_{jk} \mathcal{M}_k} \tag{7}$$

This requires the experimental determination of the stoechiometric factors - γ_{ji}, which are not directly available in the literature but may be derived from experimental studies [2–4]. For type 1 and type 2 models, the overall pyrolysis gas production may still be obtained from the same data set by summing over the production terms: $\Pi = \sum_{i=1}^{N_s} [\pi_i M_i]$. Obviously some quality information is lost during the summing process but this shows well the compatibility between type 1-2 and type 3 models and how code users can always switch back to the simplest models when in possession of type 3 data.

Type 3 models include the species conservation equation to accurately track species transport and chemical reactions within the pores of the material. The species conservation equation may be written in mass fraction - y_i as

$$\partial_t(\epsilon_g \rho_g y_i) + \partial_{\mathbf{x}} \cdot (\epsilon_g \rho_g y_i \mathbf{v_g}) + \partial_{\mathbf{x}} \cdot \mathcal{F}_i = \pi_i M_i + \epsilon_g \omega_i M_i \tag{8}$$

where, $\mathcal{F}_i$ is the diffusion flux of the i^{th} species. At low pressures, mass transfer (diffusion) in porous media is not negligible compared to convection [5]. Multi-component mass transfer in porous media is a complex problem that we treat in two steps. First, Stefan-Maxwell model is used to estimate the average bulk diffusion coefficients for each species. Then, the Bosanquet model [5] is used in a second step to account for tortuosity effects in all regimes (Knudsen to continuum). There currently is no reliable - or even well founded - finite-rate chemistry model for the homogeneous and heterogeneous reactions of pyrolysis gases (ω_i term). We use in section V a coherent model based on the reduction of a large combustion database [15] but its validation for ablative materials is still in process.

A solid-phase mass conservation model is implemented in all models to compute the effective density of the solid. The volume-averaged density change of the matrix due to pyrolysis -Π - is modeled using forms equivalent to

$$\partial_t(\epsilon_m \rho_m) = -\Pi \tag{9}$$

Coking is completely neglected in type 1 and 2 codes. Ablation and spallation are modeled as surface phenomena, so they do not appear in in-depth equations. In the proposed type 3 framework, the solid mass-conservation equation is generalized to account for in-depth heterogeneous reactions (coking, ablation [8]) and spallation

$$\partial_t(\epsilon_s \rho_s) = \partial_t(\epsilon_m \rho_m + \epsilon_f \rho_f) = -\Pi + \sum_{i \in s} \epsilon_g \omega_i M_i + \sum_{i \in s} \tau_i M_i \tag{10}$$

This overall mass balance is valid for any material. The determination of the intrinsic heterogeneous reaction rates for ablation and coking -$\omega_{i,i \in s}$- is not an easy task. The in-depth ablation and coking behaviors of the different phases depend on the microstructure of the material of interest. An original experimental technique and a modeling approach have been proposed in a preliminary study to extract the needed parameters [8]. There are two technical difficulties that are being tackled in more details and are presented in companion papers at this conference: measuring the intrinsic reaction rates at the fiber scale [16] and modeling the micro-structure and its evolution due to ablation and coking [17].

III.B. Momentum conservation in porous media

In type 2 and 3 codes, the average gas velocity is obtained by resolution of the momentum-conservation equation. In porous media, the volume-averaged momentum conservation may be written as

$$\mathbf{v_g} = -\frac{1}{\epsilon_g \mu} \frac{1+\beta/p}{1+Fo} \underline{\underline{\mathbf{K}}} \cdot \partial_{\mathbf{x}} p \tag{11}$$

Most of the materials are anisotropic, therefore, the permeability - $\underline{\underline{\mathbf{K}}}$ - is a second order tensor. For example, Fiberform, the carbon preform of PICA [18], has orthotropic permeability properties [19]. For creeping (Stokes) flows in the continuum regime (in the pores of the material), the momentum conservation degenerates into Darcy's law ($\beta = 0$, $Fo = 0$). The term $1 + \beta/p$ is the Klinkenberg correction to account for slip effects (at the pore scale) when the Knudsen number (ratio of the mean free path to the mean pore diameter) is not small. The term $1 + Fo$ is the Forchheimer correction to account for high velocity effects at the pore scale (flow separation in the continuum regime). Typically, Forchheimer effects are expected to occur for pyrolysis gas velocities higher than $50\,m/s$ (that is, in high-density ablative materials submitted to very high heat fluxes). It is not advised to use both corrections simultaneously as they address different regimes.

III.C. Energy conservation

According to Puiroux [20], solid and gas phases are in thermal equilibrium as long as the Péclet number for diffusion of heat within the pores is small ($Pe = \epsilon_g \rho_g c_{p,g} d_p v_g / k_g$). In most of the applications of interest for space agencies, the small pore size ($< 100\mu m$) and the slow pyrolysis gas flow ($v_g \sim 1m/s$) insure a small Péclet number: the gas temperature accommodates to the solid temperature within the pores [5]. Under the thermal equilibrium assumption, the energy conservation may be written as

$$\partial_t \rho_a e_a + \partial_{\mathbf{x}} \cdot (\epsilon_g \rho_g h_g \mathbf{v_g}) + \partial_{\mathbf{x}} \cdot \sum_{i=1}^{N_g} (h_i \mathcal{F}_i) = \partial_{\mathbf{x}} \cdot (\underline{\underline{\mathbf{k}}} \cdot \partial_{\mathbf{x}} T) + \mu \epsilon_g^2 (\underline{\underline{\mathbf{K}}}^{-1} \cdot \mathbf{v}) \cdot \mathbf{v} \tag{12}$$

where the total (storage) energy of the ablative material is the sum of the energy of its phases

$$\rho_a e_a = \epsilon_g \rho_g e_g + \epsilon_m \rho_m h_m + \epsilon_f \rho_f h_f \tag{13}$$

The second and third terms of the left-hand side are the energy convected (advection) and the energy transferred (diffusion) by the pyrolysis gases, respectively. Heat transfer is conveniently modeled as an effective diffusive transfer (Fourier's law). The effective conductivity - $\underline{\underline{\mathbf{k}}}$ - is a second order tensor accounting for conduction in the solid, conduction in the gas, and effective radiative heat transfer. The validity of this approach is questionable. The main issue is the validity of the linearization of the radiative heat transfer. A theoretical study has shown that radiative heat transfer may be linearized for two-dimensional carbon-fiber preforms [21,22]. The applicability to other materials and the experimental validation are not straightforward and need to be investigated but this is outside the scope of this presentation. The second term on the right-hand side is the energy dissipated by viscous effects in Darcian regime [23]. It is in general small compared to the heat transfer term.

It may seem that no major improvement is added to the momentum and energy conservation equations but they actually inherit from the detailed resolution of the mass conservation equations since the following parameters are now computed with more accuracy: viscosity, mean molar mass, porosity, permeability, enthalpies.

III.D. Boundary conditions

At the bondline, conservative boundary conditions are generally used (adiabatic and impermeable). At the surface, simple wall boundary conditions may be used for simple analyses. A popular one consists in prescribing temperature, pressure, and recession (they can change as a function of time). It is not described here because it is trivial but it is available in PATO and most codes. In ablative conditions, when the wall temperature and the surface recession are unknown, surface energy balance and surface mass balance are used as boundary conditions. This is presented below.

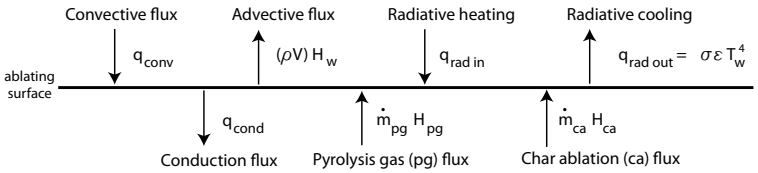

Figure 2. Energy balance at the wall

III.D.1. Surface energy balance

The surface energy balance at the wall depicted in figure 2 reads

$$q_{conv} - (\rho V)h_w + q_{rad,in} - q_{rad,out} - q_{cond} + \dot{m}_{pg}h_{pg} + \dot{m}_{ca}h_{ca} = 0 \tag{14}$$

where the convective heat flux - $q_{conv} = \rho_e u_e C'_H(h_e - h_w)$ - and the radiative heat flux are extracted from CFD simulations. The Stanton number C_H is corrected to account for the blockage induced by the pyrolysis-ablation gas-blowing; that is, the heat transfer coefficient is corrected. For example, the following correction is widely used $C'_H = C_H\, ln(1+2\lambda B')/ln(2\lambda B')$, where $B' = (\dot{m}_{pg} + \dot{m}_{ca})/(\rho_e u_e C_M)$ is a dimensionless mass flow rate and λ is a scaling factor usually taken equal to 0.5 [24]. The resolution of Eq. 14 requires the evaluation of the pyrolysis-gas flow rate - $\dot{m}_{pg}$ - and of the ablation rate - $\dot{m}_{ca}$.

III.D.2. Surface mass balance and recession rate

The pyrolysis-gas flow rate - $\dot{m}_{pg}$ - is directly obtained in the material-response code by integration of the pyrolysis, transport, and mass equations, as explained previously. However, the ablation rate - $\dot{m}_{ca}$ - is a function of both the mass transfer in the boundary layer and the thermo-chemical properties at the wall (pyrolysis-gas blowing rate and composition, temperature, pressure, boundary-layer gas composition). A common practice is to assume thermochemical equilibrium at the wall to compute the ablation rate. The model still in use in the community was developed in the sixties [25]. It is based on element conservation in steady-state in a control volume close to the wall as sketched in figure 3 and expressed in Eq. 15. The underlying hypothesis is that over a time increment Δt, the equilibrium chemistry problem in the control volume is quasi-steady (decoupling of the material response and of the boundary layer problem). This increment Δt should be at least as long as the time increment of the heat transfer simulation (material response code) but short enough so that p, T, $\dot{m}_{pg}$, and y_{pg} variations may be neglected. This is verified in typical applications. For this presentation, we shall assume equal diffusion coefficients of the elements. Failure modes (spallation, mechanical erosion) are not included and the char is assumed to be composed of a single element (for example, carbon).

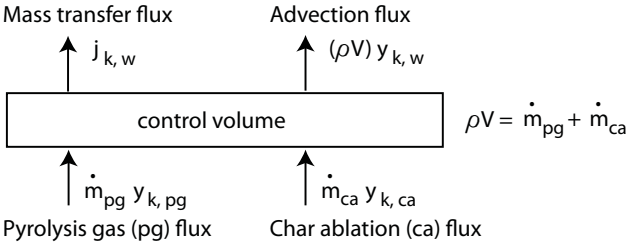

Figure 3. Element mass-fraction conservation at the wall

The inputs and outputs to this problem are:

- Inputs: $\dot{m}_{pg}$, $y_{k,pg}$, $y_{k,ca} = 1$, $y_{k,e}$, p, T.
- Outputs: $\dot{m}_{ca}$, $y_{k,w}$.

The conservation of the mass-fraction of element k in the control volume close to the wall reads:

$$j_{k,w} + (\rho V) y_{k,w} = \dot{m}_{pg} y_{k,pg} + \dot{m}_{ca} y_{k,ca} \tag{15}$$

where pg= pyrolysis gases, ca = char ablation products, w= wall (or control volume). The usual element-conservation rules apply:

- The relative mass fractions sum to 1 in each phase
  $\sum_k y_{k,w} = 1$; $\sum_k y_{k,pg} = 1$; $\sum_k y_{k,ca} = 1$
- Since p, T are fixed, the element mass-fraction conservation in the control volume is equivalent to the mass conservation.

Under the hypotheses that $Prandtl = Lewis = 1$ and that the diffusion coefficients are equal for the elements, equation 15 may be rewritten as

$$\rho_e u_e C_H (y_{k,w} - y_{k,e}) + (\rho V) y_{k,w} = \dot{m}_{pg} y_{k,pg} + \dot{m}_{ca} y_{k,ca} \tag{16}$$

where, C_H is the Stanton number and $(\rho V) = \dot{m}_{pg} + \dot{m}_{ca}$.

The formation reaction of species A_i may be written:

$$A_i \rightleftharpoons \sum_{k \in Elements} \nu_{i,k} A_k \tag{17}$$

The i chemical equilibriums read:

$$\sum_{k \in Elements} \nu_{i,k} ln(x_k) - ln(x_i) - ln(K_i) = 0 \tag{18}$$

with $x_i = 1$ if A_i is a solid species. Species mole fractions sum to one:

$$\sum_{i \in Species} x_i = 1 \tag{19}$$

To sum up, the set of equations solved is:

$$\rho_e u_e C_H (y_{k,w} - y_{k,e}) + (\rho V) y_{k,w} = \dot{m}_{pg} y_{k,pg} + \dot{m}_{ca} y_{k,ca} \tag{20}$$

$$\sum_{k \in Elements} \nu_{i,k} ln(x_k) - ln(x_i) - ln(K_i) = 0 \tag{21}$$

with $x_i = 1$ if A_i is a solid species.

$$\sum_{i \in Species} x_i = 1 \tag{22}$$

The base model may be extended when needed to account for multicomponent mass transfer, non-equal diffusion coefficients, failure (spallation, melting), a solid phase made of more than one element (example: SiO_2), heterogeneous finite-rate chemistry.

IV. Modules available in PATO, numerical method, and verification

PATO is composed of two type of modules - each of them composed of two solvers, as shown in figure 4:

- global analysis modules, that may be used to run a full ablative material response, with an applied/macroscopic scale point of view. The PAM modules are implementations of type 2 (PAM_2) and type 3 (PAM_3) material-response models, as described in the previous section and summarized in figure 4.

PATO	Global analysis modules		Elementary analysis modules	
	PAM_2	**PAM_3**	**COACO_1**	**COACO_2**
Summary				
Model fidelity (1-3)	**2**	**3**	**1**	**3**
Code dimensionality (1-3)	**3**	**3**	**1**	**3**
Code maturity level (1-3)	**3**	**1**	**3**	**1**
Gas-phase Mass Conservation	**In-depth: Eq. 1**			
Storage ($\partial_t \varepsilon_g \rho_g$)	x	x		x
Divergence ($\partial_x .(\varepsilon_g \rho_g \mathbf{v_g})$)	x	x		x
Pyrolysis production (Π)	x	x		x
Pyrolysis model	**In-depth: Eq. 2-7**			
SoA Arrhenius laws (gives Π)	x	x		
Species production (gives πi)		x		
Gas-species Conservation	**In-depth: Eq. 8**			
Storage ($\partial_t \varepsilon_g \rho_g y_i$)		x	x	x
Divergence ($\partial_x .(\varepsilon_g \rho_g y_i \mathbf{v_g})$)		x	x	x
Diffusion ($\partial_x \mathbf{F_i}$)		x	binary	multi-component
Pyrolysis species prod. ($\pi_i M_i$)		x		
Finite-rate chemistry ($\omega_i M_i$)		x	x	x
Solid-phase mass conservation	**In-depth: Eq. 9, 10**			
Pyrolyzing matrix mass loss	x	x		
In-depth ablation/coking		x	x	x
Momentum conservation	**In-depth: Eq. 11**			
Darcy's law ($\mathbf{v_g}=\mathbf{f}(\partial_x p)$)	x	x		
Klinkenberg correction		x		
Energy conservation	**In-depth: Eq. 12, 13**			
Storage ($\partial_t \rho_a e_a$)	x	x		
Divergence ($\partial_x .(\varepsilon_g \rho_g h_g \mathbf{v_g})$)	x	x		
Diffusion ($\partial_x .\Sigma(h_i \mathbf{F_i})$)	x	x		
Effective conduction (Δk)	x	x		
Viscous dissipation f(K,v)		x		
Boundary conditions	**At the wall: Eq. 14-22**			
Prescribed pressure (p(t))	x	x		
Prescribed temperature (T(t))	x	x	x	x
Surface energy balance (Q)	x	x		
Boundary layer approx. (B')	x	x		
Fixed species concentration		x	x	x
Other utilities	**Integrated libraries**			
Equilibrium chemistry solver		Mutation++		
Finite-rate chemistry solver		Mutation++		
Uncertainty analysis		Dakota (2014)		
Automatic mesh generation	1D, 2D IsoQ wedge, 3D cylinder	1D, 2D IsoQ wedge, 3D cylinder		

Figure 4. Summary of the capabilities of PATO's modules

- elementary analysis modules, that may be used to study specific fundamental aspects, with a detailed/microscopic scale point of view. The modules COACO_1 and COACO_2 are specifically developed to analyze carbon oxidation experiments and extract intrinsic reaction rates of carbon fibers.

They are also used to test and validate volume-averaged fiber oxidation models, needed for PAM_3 (equation 10) [8].

PATO is a fully portable OpenFOAM-extend library. OpenFOAM is an open-source finite-volume computational-fluid-dynamic code. Therefore, PATO uses the finite-volume method as well. To offer a more flexible modeling environment, equations are solved sequentially (as opposed to block-matrix resolution) at each time step. Each equation is solved implicitly and first-orders schemes (in time and space) are used by default as they have been found to be sufficiently accurate. The schemes can however be modified by the user at run time whenever needed. This is an OpenFOAM functionality that is inherited when using sequential solvers. All well known schemes up to 2nd order are available in OpenFOAM. There are three benefits to the sequential approach that are very useful for an analysis toolbox: 1) each equation is easily modified without impacting the stability of the whole solver, 2) independent numerical schemes may be tested for each term of each equation at execution time, 3) more equations can easily be added in the sequence to test new models. Mutation++ [26] is used as a third party library to compute all chemistry and transport related data, and for the surface mass balance in chemical equilibrium.

The individual verification of PATO operators is straightforward. OpenFOAM provides an extensive set of discretization algorithms and numerical schemes that are systematically verified by OpenCFD. However, it is still useful to verify that OpenFOAM modules are correctly used in PATO. Verifications of the time-dependent heat-transfer and momentum equations have been carried out by comparison with analytical solutions and with a commercial CFD tool (FlexPDE, www.pdesolutions.com). For the overall verification of the PAM modules, several ablation test-cases have been specifically designed to allow rigorous material-response code comparisons. The effort was started in 2011 to allow comparisons of ablative material response codes and models in an open forum. Since then, two test-case series have been proposed within the framework of the NASA/AFOSR/SNL ablation workshop - around February, each year [27, 28]. In 2013, the third test-case series was presented at the Gordon Research Conference on Atmospheric entry (8-12 February 2013) [29]. The test-case series are designed to propose problems of increasing complexity. Each series tackles only a few aspects of the material response to allow a targeted comparison of the codes and of the models. The first test-case was mostly a heat transfer problem chosen for its simplicity, allowing to set the focus on the in-depth material response [27]. The second test-case series went one step further and made use of a convective boundary condition - as in state-of-the-art design codes [28]. The main goal of the third series is to test the 2D-axisymmetrical and 3D modeling capabilities of the participating codes and assess multidimensional effects [29]. PATO was one of the codes used to design the three test-case series, together with FIAT [24] (series 1), MOPAR [30] (series 1, 2), Amaryllis [31] (series 2, 3). Extensive comparisons of PATO/PAM_2 with FIAT (series 1), MOPAR (series 1 and 2), and Amaryllis (series 1, 2) have been done with an excellent agreement. All test cases are included in the tutorials distributed with PATO releases. We present here a comparison for the most elaborated and well defined test-case at this time, which is test-case 2.3. In summary, test-case 2.3 consists in a 5 cm uni-dimensional sample of TACOT (Theoretical Ablative Composite for Open Testing [27]) heated on one side by a convective air heat flux at atmospheric pressure for one minute followed by a cool down phase of one minute. For a complete description of the test-case please refer to the test-case description document [27]. Figure 5 shows the comparison between Amaryllis and PATO/PAM_2 for test-case 2.3 in the format required in the test-case description document [28]. It features thermocouple-type output on the top graph, and in the bottom graph the following: pyrolysis-gas flux (in red), ablation flux (green), location of the virgin/charring zone interface (blue), location of the char/charring zone interface (purple), extend of recession (turquoise). The agreement between PATO/PAM_2 and Amaryllis is excellent for all data.

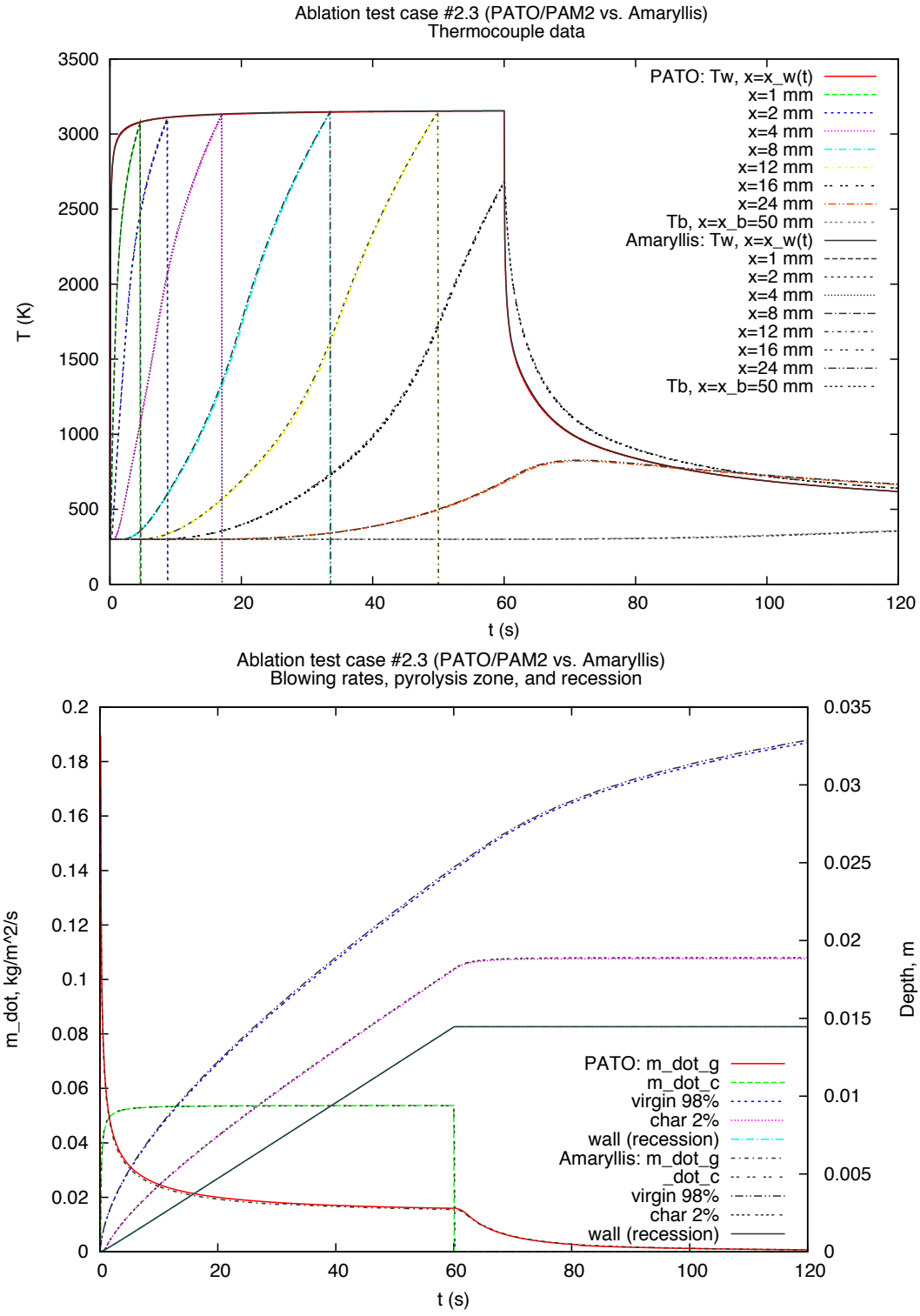

Figure 5. Ablation test-case series - test-case 2.3: comparison of PATO/PAM_2 and Amaryllis (type 2).

V. Applications

The applications presented below are part of the tutorials distributed in PATO releases. Three applications are presented: an elementary analysis with COACO_1, a multi-dimensional analysis with PAM_2, a high-fidelity analysis with PAM_3.

V.A. Analysis of the oxidation of a carbon preform in a flow-tube reactor with COACO_1

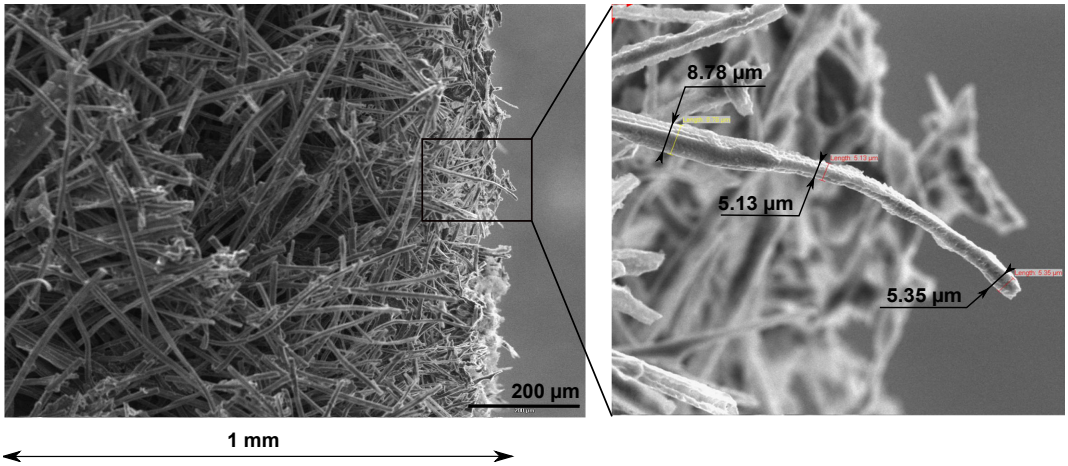

Figure 6. Scanning electron micrographs of the exposed side of the FiberForm cylinder. On this figure, the dry air flow (898K, 1013hPa) comes from the left. The fibers in the first millimeter are progressively oxidized showing a reduction of their diameter. It is a typical in-depth oxidation mechanism with a diffusion/reaction competition. COACO_1 has been used to analyze this test and extract the intrinsic reaction rate of the carbon-fibers.

The first application proposed has been presented in details in the following paper: "Validation of a volume-averaged fiber-scale model for the oxidation of a carbon-fiber preform" [8]. We will summarize here the main findings and COACO_1 results. Readers interested in more details are kindly asked to refer to the original publication. The objective of this work was to analyze the oxidation mechanism of a carbon-fiber preform and obtain its effective reaction rate in order the provide data for the equation 10 of type 3 models. The oxidation of FiberForm, an industrial carbon-fiber preform, was studied in a tubular oxidation reactor at 898K; dry air at 898K and 1013 hPa was blown through a cylindrical plug snuggle-fit in a quartz tube. The microscopic oxidation behavior of the fibers was analyzed by scanning electron microscopy after test. The carbon fibers clearly oxidize via a progressive reduction of their diameter. The overall material recession occurs when the fibers are consumed. It was obvious that a reaction/diffusion-convection competition had driven the oxidation process and controlled the depth of oxidation (figure 6). Using COACO_1 it is possible to infer the intrinsic reactivity of the carbon fibers from the knowledge of the depth of oxidation. Indeed, since the diffusion coefficients are known variables, the only unknown in the reaction/diffusion competition problem was the intrinsic fiber reactivity (that controls the depth of oxidation). COACO_1 results are shown and commented in figure 7.

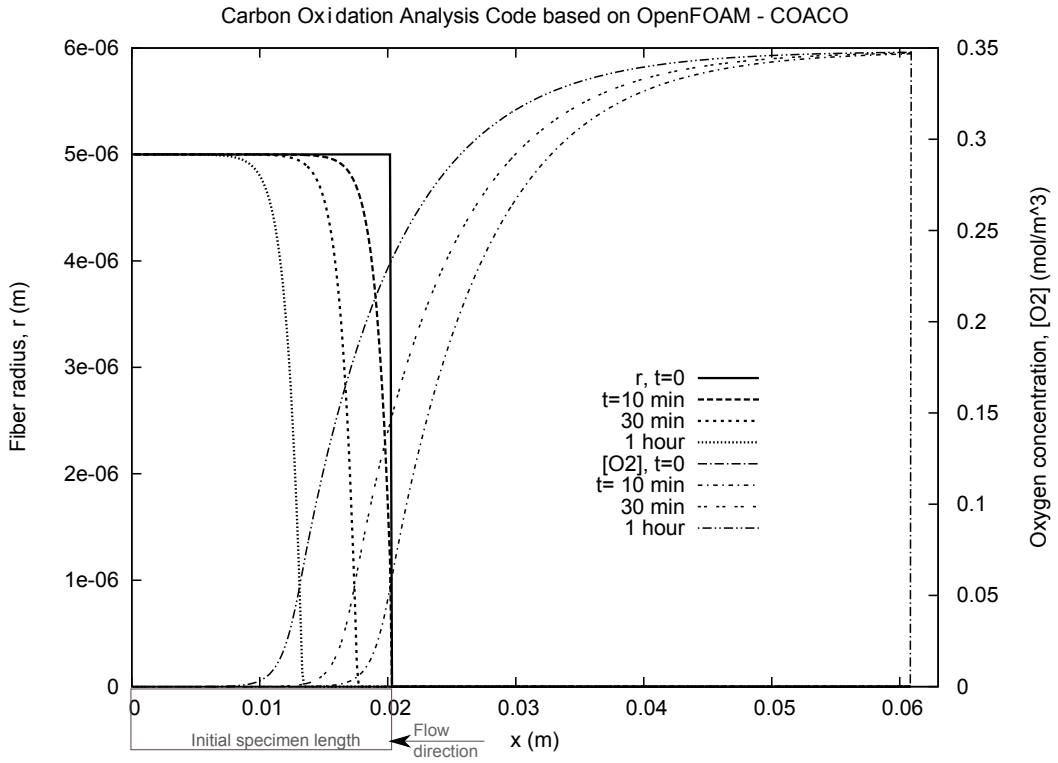

Figure 7. COACO_1 simulation of the time-dependent oxidation of a carbon-fiber preform used to extract the intrinsic reactivity of the carbon fibers. The simulation shown the progressive reduction of the mean fiber radius, the overall sample recession, and the oxygen concentration in the reactor (that drops quickly as it diffuses into the carbon-fiber preform due to the reaction-diffusion competition).

V.B. Analysis of the pyrolysis-gas flow and heat transport in a 3D cylinder facing an ArcJet with PAM_2

This example presents a purely theoretical case aiming at showing the 3D capabilities of PATO and the interest of type 2 codes that can compute the direction of the pyrolysis-gas flow. A cylinder of TACOT is heated for 40 seconds by a mini Arc Jet with a stagnation region small compared to the size of the sample. The cylinder has impermeable walls on the sides and at the bottom. The following conditions were arbitrarily chosen for the heat load at the stagnation point: 3 MW/m^2, recovery enthalpy= 10 MJ/kg, p= 1013 hPa, air, and a gaussian decay was used along the radial direction. The case has been studied with PATO/PAM_2. We show and analyze results after 40 seconds of heating. Figures 8 and 9 show the ablation profile, the temperature and pressure contours, and the pyrolysis-gas flow. A well defined hot zone develops in the center of the sample. The internal pressure that builds up below the hot zone generates a fully multidimensional pyrolysis gas flow. A fraction of the pyrolysis-gas goes down first and then escapes from outside the hot zone. Therefore, such a problem is typically not mono-dimensional - even in its center - and needs to be analyzed with a multi-dimensional code that models the gas flow direction (type 2 model).

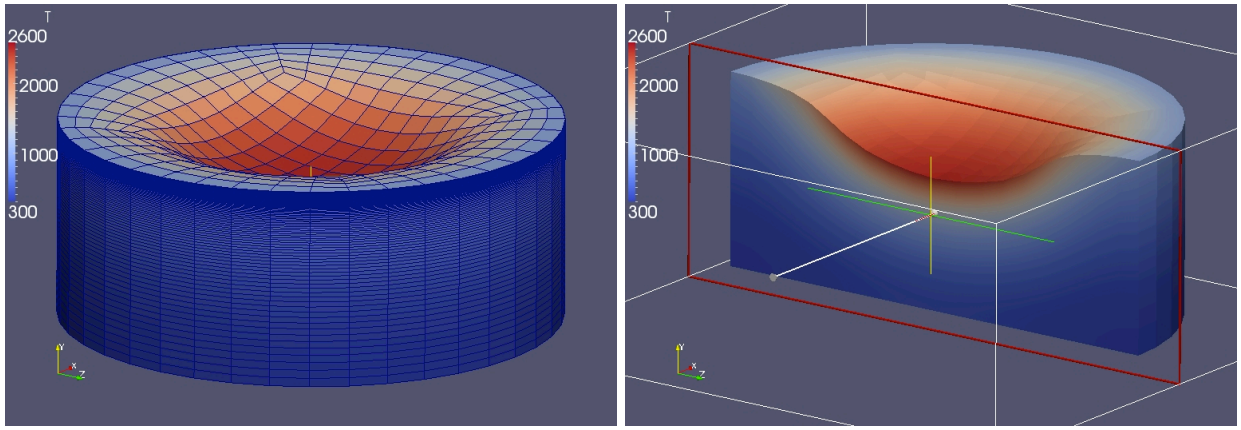

Figure 8. Cylindrical sample of TACOT after 40 seconds under micro-ArcJet conditions - stagnation conditions: flux: 3 MW/m^2, recovery enthalpy= 10 MJ/kg, p= 1013 hPa, air. Material response computed with PAM_2: temperature contours.

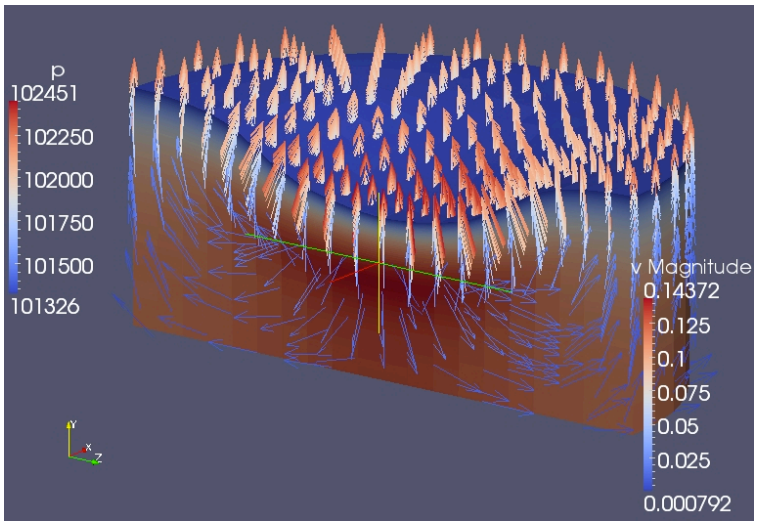

Figure 9. Cylindrical sample of TACOT after 40 seconds under micro-ArcJet conditions - stagnation conditions: flux: 3 MW/m^2, recovery enthalpy= 10 MJ/kg, p= 1013 hPa, air. Material response computed with PAM_2: pressure contours and pyrolysis-gas velocity vectors.

V.C. Finite-rate chemistry effects on temperature profile and gases injected in the boundary layer

We propose here a simple application to show finite-rate chemistry effects. We use as a support the ablation test-case 1.0 [27] and compare type 1, type 2, and type 3 code results. Test-case 1.0 is unidimensional. As shown in figure 10, a sample of TACOT of 5 cm is heated on one side at 1664K for 1 minute at atmospheric pressure and cooled down by re-radiation for 1 minute. Adiabatic boundary condition are used at the bottom. The initial conditions are: p= 1atm (101325 Pa), T= 300K, sample length: 0.05 m. The initial gas composition in the material is left open. We use pyrolysis gases at equilibrium for the type 2 model because this is the usual practice. We use dry air for the finite-rate chemistry case because it makes more sense. The type 2 model used is the one presented in the ablation test-case document and in the TACOT definition file [27]. We believe that the finite-rate chemistry models initially proposed in the TACOT definition file can be significantly improved. Therefore, we use here what we think is a better set of data. The high-fidelity pyrolysis model provided in table 1 and derived from literature data is used.

j	Pyrolysis balance equations	Peak (K)	F_j	A_j	E_j	m_j	n_j
	Model (Sykes [2]/Goldstein [11]/Trick [3, 4])	S./T.	S.	G.	G.	G.	G.
1	$PM_1 \rightarrow H_2O\,(physisorbed)$	373	0.01	$8.56 \cdot 10^3$	$7.12 \cdot 10^4$	3	0
2	$PM_2 \rightarrow 0.69\,H_2O + 0.01C_6H_6$ $+0.01C_7H_8 + 0.23C_6H_6O$	773	0.24	$8.56 \cdot 10^3$	$7.12 \cdot 10^4$	3	0
3	$PM_3 \rightarrow 0.09\,CO_2 + 0.33\,CO + 0.58\,CH_4$	873	0.03	$4.98 \cdot 10^8$	$1.70 \cdot 10^5$	3	0
4	$PM_4 \rightarrow H_2$	1073	0.06	$4.98 \cdot 10^8$	$1.70 \cdot 10^5$	3	0
5	$PM_5 \rightarrow C$	$--$	0.66	0	0	3	0

Table 1. Pyrolysis balance equations and kinetic parameters.

A reduced 22-species homogeneous finite-rate chemistry mechanism derived from the combustion database of Blanquart [15] is used for the homogenous chemistry of the pyrolysis gases. The list of species is shown in figure 14. We do not provide the complete mechanism as it lacks validation in the context of ablative materials. It is still used here because there is no other well funded mechanism available in the literature for our application. The first graph (figure 11) shows the excellent agreement between PATO/PAM2 and FIAT (type 1), showing that in this simple configuration type 1 and type 2 codes provide similar results - as discussed in section III. Figure 12 shows a comparison of the thermal response when using finite-rate chemistry versus equilibrium chemistry. The difference is explained by the fact that the pyrolysis gas enthalpies are significantly different (equilibrium vs. finite-rate), as shown in figure 13. Figure 14 shows the evolution of the pyrolysis gas composition as it is convected through the material towards the surface - in the absence of diffusion here. It is obvious that in this case the finite-rate chemistry model used in the material will have a strong influence on the predicted species in the boundary layer and that the equilibrium assumption would not be correct. It is interesting to note that a large amount of benzene (A1) is injected in the boundary layer according to the finite-rate chemistry model used whereas benzene is not even present when using equilibrium chemistry. Of course, the results presented here only have a qualitative value because a validation of the combustion-database chemistry mechanism in the context of ablative materials is still needed.

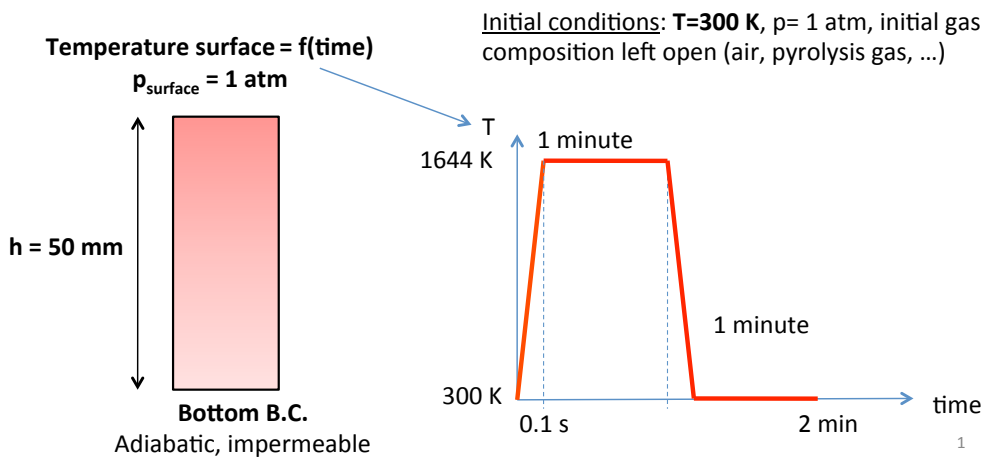

Figure 10. Schematic description of test-case 1.0

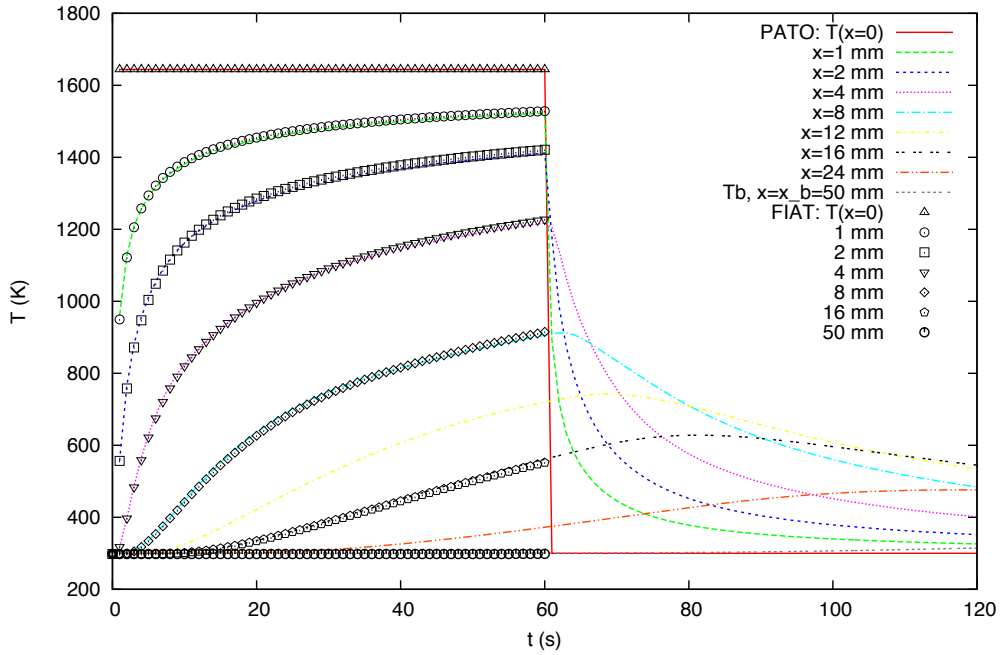

Figure 11. Test-case 1.0: comparison of thermal response between PATO/PAM2 and FIAT

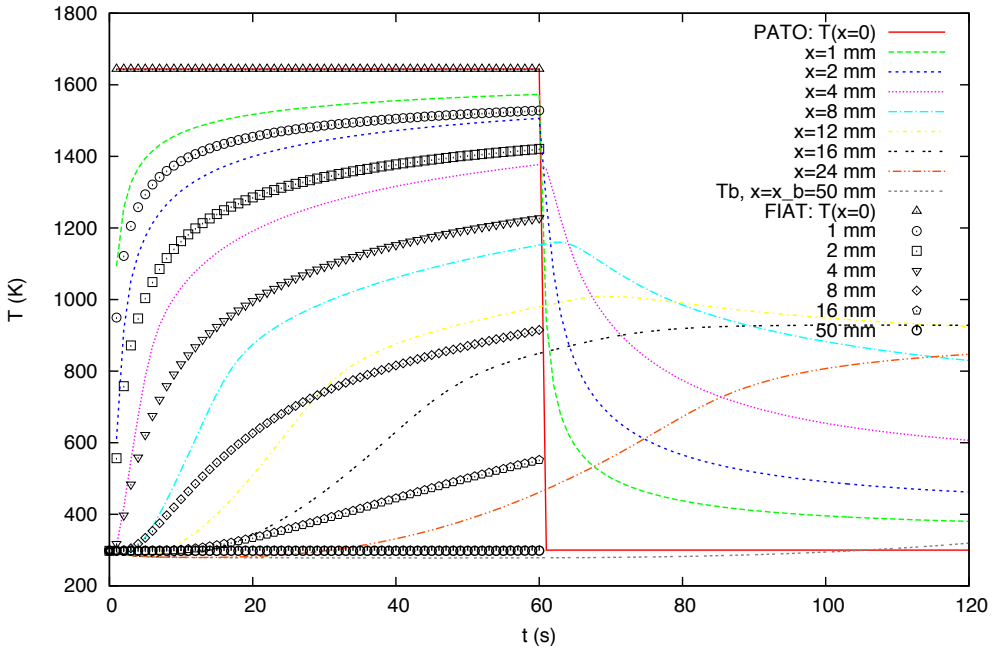

Figure 12. Test-case 1.0: comparison of thermal response between PATO/PAM3 and FIAT

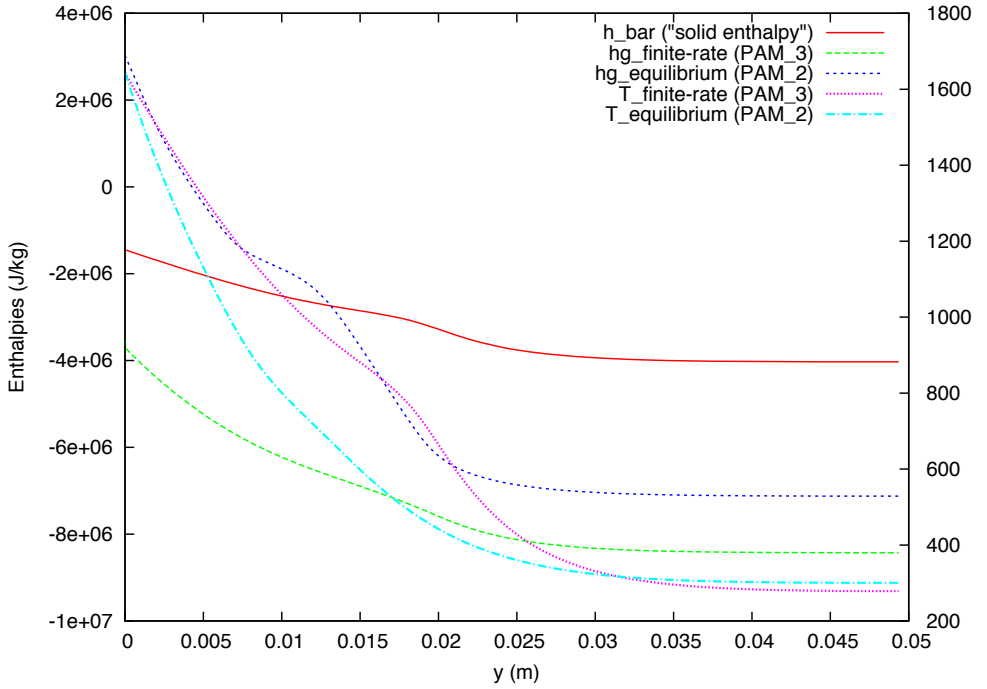

Figure 13. Test-case 1.0: comparison of temperature and enthalpy profiles (the temperature scale is on the right)

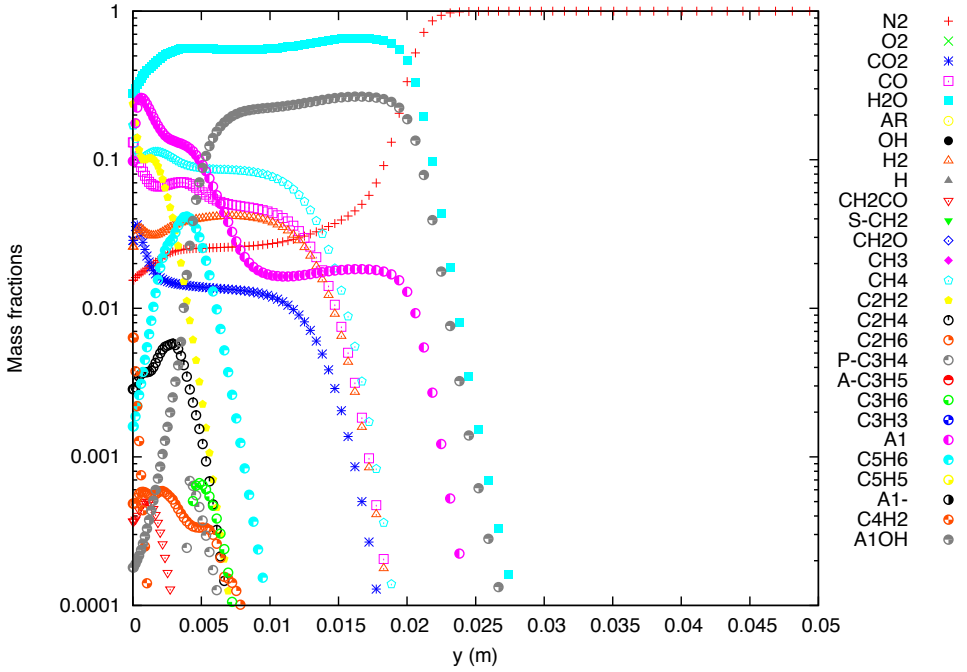

Figure 14. Test-case 1.0: PATO/PAM3 - Blanquart 22 species - diffusion neglected

VI. Conclusion

The Porous-material Analysis Toolbox based on OpenFOAM-extend (PATO) is composed of two type of modules - each of them composed of two solvers:

- global analysis modules, that may be used to run a full ablative material response, with an applied/macroscopic scale point of view. The PAM modules are implementations of type 2 (PAM_2) and type 3 (PAM_3) material-response models.
- elementary analysis modules, that may be used to study specific fundamental aspects, with a detailed/microscopic scale point of view. The modules COACO_1 and COACO_2 are specifically developed to analyze carbon oxidation experiments and extract intrinsic reaction rates of carbon fibers. They are also used to test and validate volume-averaged fiber oxidation models.

Elementary analysis and global analysis applications have been proposed. They show how PATO complements the capabilities of current production codes. The elementary modules bring some insight on very specific problems, as illustrated here with the case of Fiberform oxidation. The global modules aim at comparing different level of models, and may be used to validate hypotheses used in production codes, as shown with the examples of the ablation test-case series (comparison of equilibrium and finite-rate chemistry) and of the 3D cylinder problem (multi-dimensionality effects, pyrolysis-gas flow effects).

PATO is available for world-wide academic release with some restrictions. The copyright is owned by NASA. Please contact the authors for more information.

Acknowledgments

This research was originally funded by NASA's Fundamental Aeronautic Program Hypersonics NRA grant NNX12AG47A, it is currently supported by the Space Technology Research Grants Program.

References

[1]Moyer, C. B. and Rindal, R. A., "An Analysis of the coupled chemically reacting boundary layer and charring ablator: Part II," *NASA CR*, Vol. 1061, 1968, 168 p.

[2]Sykes, G. F., "Decomposition characteristics of a char-forming phenolic polymer used for ablative composites," *NASA TN*, Vol. D-3810, 1967, 20 p.

[3]Trick, K. A. and Saliba, T. E., "Mechanisms of the pyrolysis of phenolic resin in a carbon/phenolic composite," *Carbon*, Vol. 33, No. 11, 1995, pp. 1509–1515.

[4]Trick, K. A., Saliba, T. E., and Sandhu, S. S., "A kinetic model of the pyrolysis of phenolic resin in a carbon/phenolic composite," *Carbon*, Vol. 35, No. 3, 1997, pp. 393–401.

[5]Lachaud, J., Cozmuta, I., and Mansour, N. N., "Multiscale Approach to Ablation Modeling of Phenolic Impregnated Carbon Ablators," *Journal of Spacecraft and Rockets*, Vol. 47, No. 6, 2010, pp. 910–921.

[6]Lachaud, J. and Mansour, N. N., "Microscopic scale simulation of the ablation of fibrous materials," AIAA paper 2010-984, 2010.

[7]Whitaker, S., *The method of volume averaging*, Kluwer Academic Publisher, Dordrecht, The Netherlands, 1999.

[8]Lachaud, J., Mansour, N. N., Ceballos, A., Pejakovic, D., Zhang, L., and Marschall, J., "Validation of a volume-averaged fiber-scale model for the oxidation of a carbon-fiber preform," AIAA Paper 2011-2223, 2011.

[9]Lachaud, J., Magin, T., Cozmuta, I., and Mansour, N. N., "A short review of ablative material response models and simulation tools," *7th Aerothermodynamics Symposium*, edited by E. S. Agency, No. to appear, Brugge, Belgium, May 2011, 8 p.

[10]Kendall, R. M., Bartlett, E. P., Rindal, R. A., and Moyer, C. B., "An Analysis of the coupled chemically reacting boundary layer and charring ablator: Part I," *NASA CR*, Vol. 1060, 1968, 96 p.

[11]Goldstein, H. W., "Pyrolysis kinetics of nylon 6-6, phenolic resin, and their composites," *Journal of macromolecular science, Part A*, Vol. 3, No. 4, 1969, pp. 649–673.

[12]Mansour, N. N., Lachaud, J., Magin, T. E., de Muelenaere, J., and Chen, Y.-K., "High-Fidelity Charring Ablator Thermal Response Model," AIAA Paper 2011-3124, 2011.

[13]Ladacki, M., Hamilton, J. V., and Cohz, S., "Heat of pyrolysis of resin in silica phenolic ablator," *AIAA Journal*, Vol. 4, 1966, pp. 1798–1802.

[14]Laub, B., "High-fidelity model," *Tutorial on ablative TPS*, Second International Planetary Probe Workshop, NASA Ames Research Center, August 21-22, 2004.

[15]Blanquart, G., Pepiot-Desjardins, P., and Pitsch, H., "Chemical mechanism for high temperature combustion engine relevent fuels with emphasis on soot precursors," *Combust. Flame*, Vol. 156, 2009, pp. 588–607.

[16]Panerai, F., Martin, A., Mansour, N. N., Sepka, S. A., and Lachaud, J., "Flow-tube oxidation experiments on the carbon preform of PICA," 44th AIAA Thermophysics Conference, June 2013, San Diego, California.

[17]Mansour, N. N., Panerai, F., Martin, A., Parkinson, D. Y., MacDowell, A., Fast, T., Vignoles, G. L., and Lachaud, J., "A new approach to light-weight ablators analysis: from micro-tomography measurements to statistical analysis and modeling," 44th AIAA Thermophysics Conference, June 2013, San Diego, California.

[18]Tran, H. K., Johnson, C. E., Rasky, D. J., Hui, F. C. L., Hsu, M.-T., Chen, T., Chen, Y. K., Paragas, D., and Kobayashi, L., "Phenolic Impregnated Carbon Ablators (PICA) as Thermal Protection Systems for Discovery Missions," Tech. Rep. 110440, NASA Technical Memorandum, 1997.

[19]Marschall, J. and Milos, F. S., "Gas permeability of rigid fibrous refractory insulations," *Journal of Thermophysics and Heat Transfer*, Vol. 12, 1998, pp. 528–535.

[20]Puiroux, N., Prat, M., and Quintard, M., "Non-equilibrium theories for macroscale heat transfer: ablative composite layer system," *International Journal of Thermal Sciences*, Vol. 43, 2004, pp. 541–554.

[21]van Eekelen, T. and Lachaud, J., "Radiation heat-transfer model for the ablation zone of low-density carbon-resin composites," AIAA paper 2010-4904, 2010.

[22]van Eekelen, T. and Lachaud, J., "Numerical Validation of an Effective Radiation Heat Transfer Model for Fiber Preforms," *Journal of Spacecraft and Rockets*, Vol. 48, No. 3, May-June 2011, pp. 534–537, Engineering note.

[23]Ene, H. J. and Sanchez-Palencia, E., "On Thermal Equation for Flow in Porous Media," *International Journal of Engineering Science*, Vol. 20, 1982, pp. 623–630.

[24]Chen, Y. K. and Milos, F. S., "Ablation and thermal response program for spacecraft heatshield analysis," *Journal of Spacecraft and Rockets*, Vol. 36, No. 3, 1999, pp. 475–483.

[25]Moyer, C. B. and Wool, M. R., "Aerotherm Equilibrium Surface Thermochemistry Computer Program - Version 3," Tech. rep., Aerotherm, April 1970, AD875385.

[26]Scoggins, J. and Magin, T., "Multicomponent Thermodynamic And Transport property library for Ionized plasmas and applications," 44th AIAA Thermophysics Conference, June 2013, San Diego, California. 13p.

[27]Lachaud, J., Martin, A., Cozmuta, I., and Laub, B., "Ablation workshop test case - Version 1.1 - Feb. 2, 2011," Prepared for the 4th Ablation Workshop (1-3 March 2011, Albuquerque, New Mexico).

[28]Lachaud, J., Martin, A., van Eekelen, T., and Cozmuta, I., "Ablation test-case series #2," Version 2.8, Jan. 2011, 8 p., prepared for the 5th Ablation Workshop, Feb. 28-March. 1, Lexington, Kentucky.

[29]van Eekelen, T., Martin, A., Lachaud, J., and Cozmuta, I., "Ablation test-case series #3," Version1.3, Nov, 2012, 12 p.; first version presented at the 5th Ablation Workshop, Feb. 28-March. 1, Lexington, Kentucky.

[30]Martin, A. and Boyd, I., "Simulation of pyrolysis gas within a thermal protection system," AIAA paper 2008-3805, 2008.

[31]van Eekelen, T., Bouilly, J.-M., Hudrisier, S., Dupillier, J.-M., and Aspa, Y., "Design and Numerical Modelling of Charring Material Ablators for Re-Entry Applications," *Proceedings of the Sixth European Workshop on Thermal Protection Systems and Hot Structures*, European Space Agency - WPP-319, University Stuttgart, Germany, 21-25 November 2009.